

# Non-linear assessment of cold water pipe (CWP) on the ocean thermal energy conversion (OTEC) installation under bending load

**Adie, Prayoga Wira; Prabowo, Aditya Rio; Muttaqie, Teguh; Adiputra, Ristiyanto; Muhayat, Nurul; Carvalho, Hermes; Huda, Nurul**

*Published in:*
Procedia Structural Integrity

*Link to article, DOI:*
10.1016/j.prostr.2023.07.005

*Publication date:*
2023

*Document Version*
Publisher's PDF, also known as Version of record

Available online at www.sciencedirect.com

ScienceDirect

Procedia Structural Integrity 47 (2023) 142–149

Structural Integrity Procedia

www.elsevier.com/locate/procedia

27th International Conference on Fracture and Structural Integrity (IGF27)

# Non-linear assessment of cold water pipe (CWP) on the ocean thermal energy conversion (OTEC) installation under bending load

Prayoga Wira Adie[a], Aditya Rio Prabowo[a,*], Teguh Muttaqie[b], Ristiyanto Adiputra[b], Nurul Muhayat[a], Hermes Carvalho[c], Nurul Huda[d]

[a] *Department of Mechanical Engineering, Universitas Sebelas Maret, Surakarta 57126, Indonesia*
[b] *Research Center for Hydrodynamics Technology, National Research and Innovation Agency (BRIN), Surabaya 60117, Indonesia*
[c] *Department of Structural Engineering, Federal University of Minas Gerais, Belo Horizonte 31270-901, Brazil*
[d] *National Institute of Aquatic Resources, Technical University of Denmark, Lyngby 2800, Denmark*

**Abstract**

The Ocean Thermal Energy Convention (OTEC) is a floating platform that functions to convert seawater heat energy into electricity. Cold sea water is taken from the sea with a depth of 800 – 1000 m through Cold Water Pipe (CWP). This long CWP size causes unavoidable bending loads due to seawater flow. The extreme diameter/thickness ratio of CWP makes this pipe susceptible to buckling. In this research, numerical validation and mesh convergence study was carried out for CWP OTEC research under the next bending load. The results of numerical validation show that the similarity of this study with the reference reaches 15%. Dissimilarity can be influenced by different material inputs. The results of the mesh convergence study show that a mesh size of 55 mm is suitable for future research. This is because the 55 mm mesh size has results that are not much different from the smaller mesh size, but has a much smaller number of elements compared to the smaller mesh size.



*Keywords:* OTEC; CWP; Buckling phenomenon; Bending load; Numerical analysis

* Corresponding author. Tel.: +62-271-632-163; fax: +62-271-632-163.
*E-mail address:* aditya@ft.uns.ac.id (A.R.P.)


10.1016/j.prostr.2023.07.005

## 1. Introduction

The sea has a lot of renewable energy potentials (Prabowo and Prabowoputra, 2020; Prabowoputra et al., 2020a-c; Arifin et al., 2020; 2022; Prabowoputra and Prabowo, 2022), which one of them is ocean thermal energy. Ocean thermal energy can be extracted using the Ocean Thermal Energy Convention (OTEC) technology. This OTEC takes advantage of the difference in the temperature of the hot sea surface and the temperature of the cold deep seawater. The temperature difference must be greater than 20 °C. In general, OTEC is placed on a floating platform like a ship. The thermodynamic cycle in OTEC is the Rankine cycle using ammonia working fluid (Engels and Zahibian, 2014). The Rankine cycle in OTEC can be seen in Figure 1a. At this time, OTEC is still not widely used because of its small efficiency. However, there are already several OTEC installations in the world, such as an OTEC with a capacity of 100 kW on Nauru Island (Liu, 2018).

Cold seawater is taken using a Cold Water Pipe (CWP). Because cold water is taken from the deep sea, the cold water flow rate affects the power output that is released at OTEC. The greater the capacity of an OTEC, the greater the CWP. Usually, the diameter of the pipe used to take cold water at OTEC with a power of 100 MW reaches 10 m. Even though it has a large diameter, the thickness of the pipe is very small compared to its diameter. Usually, the thickness of this pipe is only 1 cm. The length of this CWP can reach 800-1000 m because it takes cold water that is 800-1000 m below sea level (Adiputra et al., 2020). The CWP is installed on the OTEC platform in a hanging manner so that one side is attached to the platform and the other side is free. The OTEC scheme is displaced in Figure 1b.

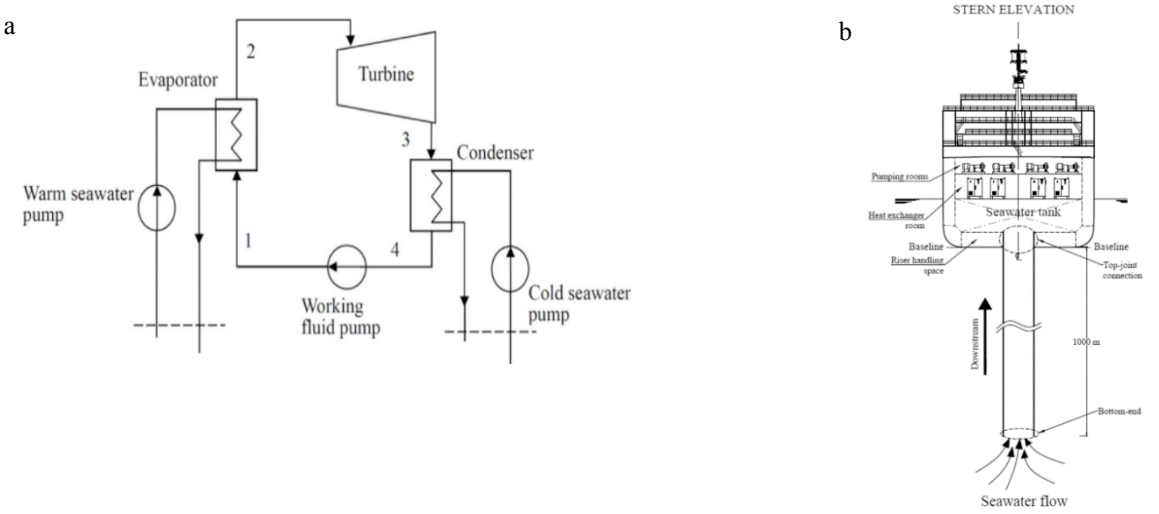


Figure 1. Illustration of the OTEC: (a) Rankine cycle (Yang and Yeh, 2014); and (b) working scheme (Adiputra and Utsunomiya, 2019).

Due to the CWP hanging, the CWP will experience a bending load because there is a flow of seawater around it. This bending load will cause buckling which is one of the failures in the structure. CWP is very susceptible to this buckling. This is due to its extreme geometry, such as its long size and very large diameter-to-thickness ratio ($D/t$).

## 2. Previous study about buckling

Research on the buckling phenomenon has existed since 1961. Tymoshenko and Gere investigated pipes subjected to axial compression loads (Timoshenko and Gere, 1961). Based on this research they found that the critical stress of a long pipe that both ends are suspended as Equation 1.

$$\sigma_{cr} = \frac{E\,t}{r\sqrt{3(1-\nu^2)}} \tag{1}$$

Where $\sigma_{cr}$ is the critical stress, $E$ is Young's modulus, $t$ is the pipe thickness, $r$ is the pipe radius, and $\nu$ is the Poisson's ratio. For a cylindrical pipe with a thin wall subjected to a bending moment load, the maximum stress

equation can be seen in Equation 2.

$$\sigma_{cr} = \frac{M}{\pi r^2 t} \tag{2}$$

$M$ is the applied moment load. If it is assumed that a pipe with a thin pipe wall is loaded with buckle bending when the compression stress reaches a value where the stress reaches buckling failure, then the critical moment can be found by combining Equations 1 and 2. If it is assumed that the material used is steel with a Poisson ratio of 0.3, then Equation 3 is obtained (Polenta et al., 2015).

$$M_{cr} = \sigma_{cr}\, \pi\, r^2\, t = 0.605\, \pi\, E\, r^2\, t \tag{3}$$

where $M_{cr}$ is the critical moment. The value of 0.605 can vary, depending on the approach. In previous studies, this value was in the range of 0.55 to 1.3. As another example, the research results from Yudo and Yoshikawa found the equation of the critical moment in Equation 4 (Yudo and Yoshikawa, 2015).

$$M_{cr} = 0.666\, \pi\, E\, r^2\, t \tag{4}$$

The approaches that have been carried out by previous research can only be used as a reference, and cannot be used as a strength value in an actual structure. This is because the critical moment is greatly influenced by the pipe geometry, especially the $D/t$ ratio. To find the buckling moment in the plastic area, Equation 5 can be used (Jay et al., 2016).

$$M_p = \left(1.05 - \frac{0.0015D}{t}\right) \sigma_Y D^2\, t \tag{5}$$

$M_p$ is the plastic moment and $\sigma_Y$ is the yield stress. In buckling pipes, there must be ovalization that occurs. Ovalization is a change in the cross-sectional shape of the pipe which was originally circular to become oval in shape due to buckling. Ovalization can reduce the value of the critical moment of a structure. The oval deformation scheme can be seen in Figure 2.

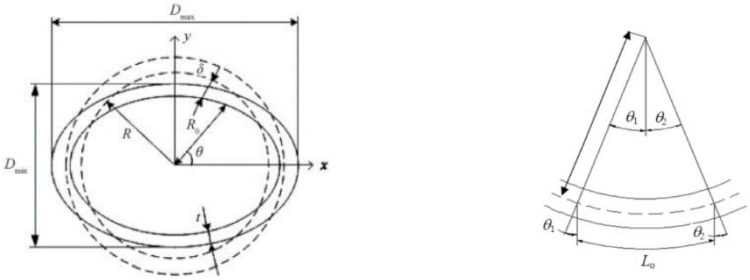


(a) (b)

Figure 2. Analytical concepts in this work: (a) Oval deformation (Li et al., 2022); and (b) Curvature (Lee et al., 2014).

The oval deformation has a non-linear curve between the moment and the curvature of the pipe. The relationship between moment and pipe curvature can be seen in Equation 6.

$$\sigma_{cr} = E\, I\, (M)\, \frac{d^2u}{dx^2} \tag{6}$$

$d^2u/dx^2$ in the Equation 6 is the curvature that occurs.

## 3. Finite Element Setting

Yadav and Gerasimidis (2019) investigated the instability of a cylindrical shell when a bending load was applied. They used a pipe with a length of 20 meters and a diameter of 4 meters. In that study, the variations used were the radius/thickness ratio (*R/t*), the shape of the imperfections (Adiputra et al., 2023), the magnitude of the imperfections, and the Ramberg-Osgood plasticity model. The boundary condition is that one end of the pipe is given rotation and the other end is a fixed end. For the current study, the model from Yadav and Gerasimidis was reproduced for future research. In this study, the *R/t* ratio used was 60, using a modal shape imperfection model with an imperfection magnitude ($w_0/t$) of 0.1, and using Ramberg-Osgood plasticity. The geometry of this model can be seen in Figure 3.

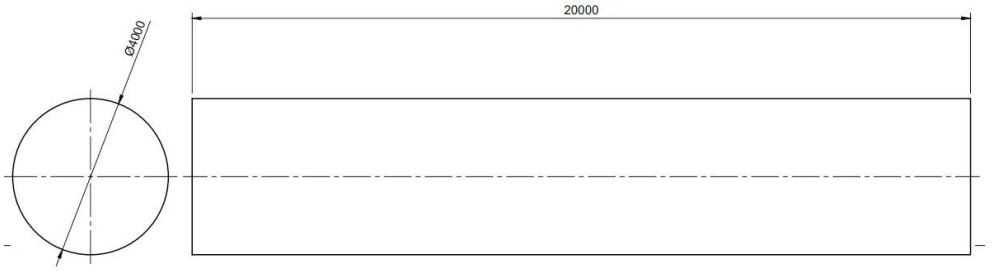


Figure 3. Yadav dan Gerasimidis geometri model (in mm).

The material used for this model is steel. The steel has a yield strength of 355 MPa, young's modulus of 210 GPa, and Poisson's ratio of 0.3. In this model, the Ramberg-Osgood plasticity model is used. For the Ramberg-Osgood model equation for steel, the mathematical form is presented in Equation 7 (Kyriakides et al., 2008).

$$\varepsilon = \frac{\sigma}{E}\left[1 + \frac{3}{7}\left(\frac{\sigma}{\sigma_y}\right)^{n-1}\right] \tag{7}$$

where $\varepsilon$ is the strain, $\sigma$ is the stress, $\sigma_y$ is the yield stress, and $n$ is the variable for the Ramberg-Osgood equation. The value of $n$ used for this model is 9.

The boundary conditions used also follow Yadav and Gerasimidis' research. At the end of the pipe is a fixed end ($U_1$=$U_2$=$U_3$=$U_{R1}$=$U_{R2}$=$U_{R3}$=0) so there is no movement at that end. Meanwhile, at the other end, a change in rotation is given so that there is a load on that end. Boundary conditions for this work are displayed in Figure 5.

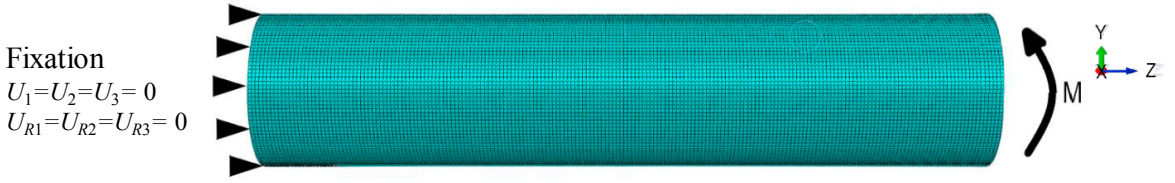


Figure 5. Boundary conditions for finite element setting.

## 4. Result and Discussion

### *4.1 Benchmarking*

In this validation, the results of the present study will be compared with the results of Yadav and Gerasimidis (2019). The results were obtained using the Static Risk method in the ABAQUS application. A comparison of the results from the reference and the present study can be seen in Figure 6 and Table 1. In these results, the moment is normalized by $M = D^2 t\sigma_y$ and curvature is normalized by $= \frac{t}{D^2}$.

Table 1. Comparison of the critical moment.

| Reference | Normalized Moment | Normalized Curvature |
|---|---|---|
| Yadav and Gerasimidis (2019) | 0.952 | 0.88 |
| Present Study | 0.985 | 1.01 |
| Difference | 3.5% | 15% |

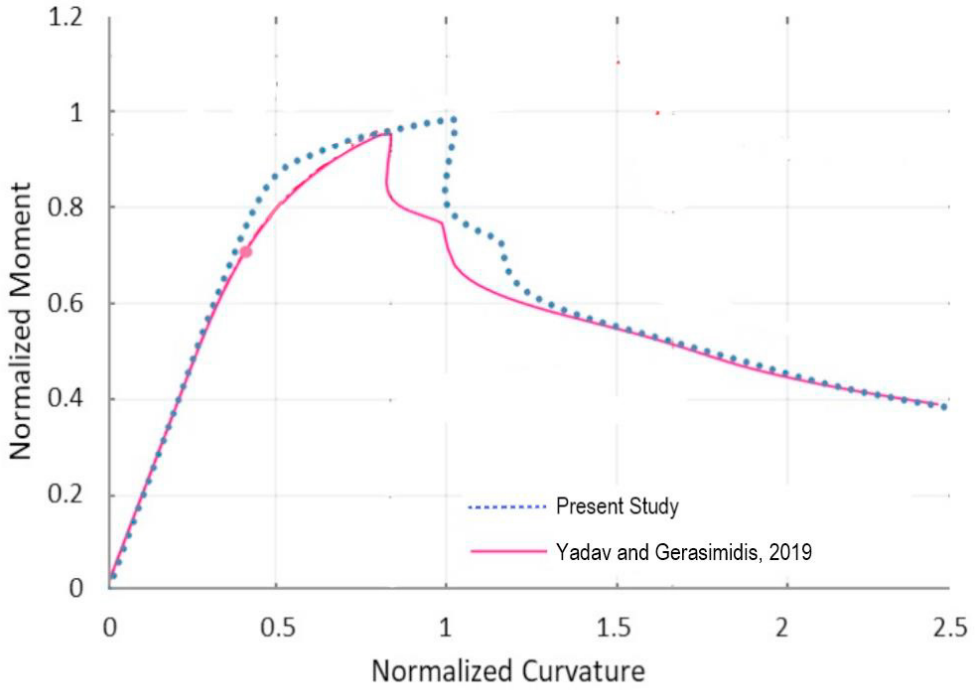


Figure 6. Numerical validation results: moment-curvature graph.

During comparison is conducted based on data in, the graph between the reference and the current study has a similar trend line (see Figure 6). The similarity is seen in the elastic part where the two curves coincide. In addition, the similarity can be seen in the post-buckling, where the two curves also coincide. However, in existing studies, there is a necking when it crosses the yield limit. In addition, the place where the critical moment occurs in the reference is earlier than the study conducted. This can be caused by differences in material input, especially during the transition between elastic and plastic deformations. In the present study, the transition between elastic and plastic deformation occurs directly, whereas, in the reference, such a phenomenon does not occur. When compared to the critical moment, it is obtained that the normalized moment is almost the same. The difference between the reference and the present study is only 3.5%. However, the difference in the normalized curvature of the reference and the present study is quite large, approximately almost 15%.

It is necessary to know the contours of the simulation results for benchmarking to know the stress propagation that occurs. The stress contours can be seen in Figure 7. Apart from that, the displacements and strains that occur in the structure can also be seen from the contours. Strain and displacement contours can be seen in Figure 8.

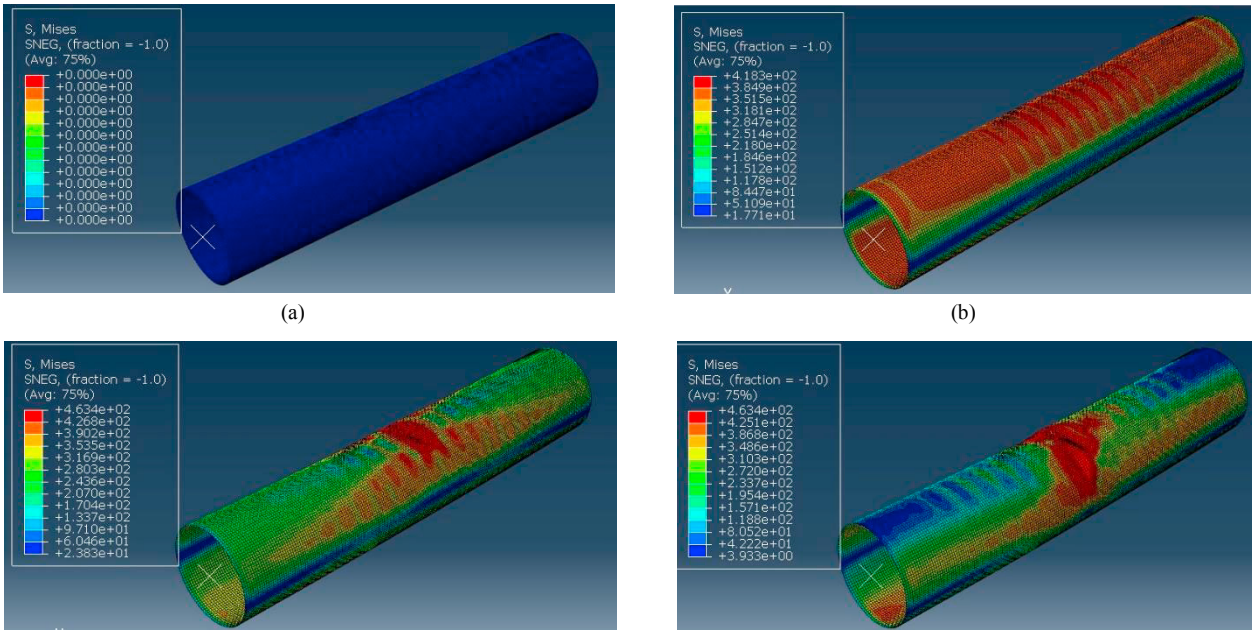


Figure 7. Stress contour based on FE analysis: (a) before loading; (b) at step 20; (c) at step 40; and (d) at step 60.

Figure 7a is a stress contour when it is not subjected to a load, so no stress occurs. When observation is continued to Figure 7b, it can be seen that the structure has undergone plastic deformation, this can be seen in the maximum stress that has exceeded the given yield strength. However, it has not yet passed its critical moment. In Figure 7c, it can be seen that the structure has passed a critical moment so that at that time the structure has failed. When it is continued, it can be seen in Figure 7d, where the failure area will get bigger. In this case, the stress propagation only occurs on one side and the direction of this propagation is unidirectional. This is because there is only one component in this structure, so the stress value does not fluctuate. As seen in Figures 7a to 7d, stress propagation only occurs in the middle of the pipe.

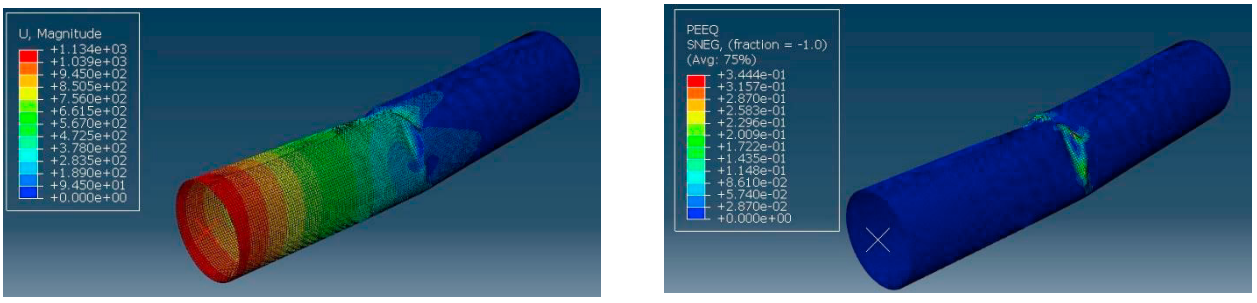


Figure 8. Contours of the FE results: (a) displacement contour; and (b) strain contour.

As depicted in Figure 8a, it can be seen that the displacement occurs in only half of the pipe. The higher the end of the pipe, the greater the displacement that occurs. This can be caused by the strain that occurs. Figure 8b shows that the strain that occurs only occurs in the middle of the pipe. Because it only occurs in the middle, then half of the pipe cannot move while the other half is lifted.

### *4.2 Mesh convergence study*

A mesh convergence study is carried out to determine the appropriate number and size of mesh for further studies. The results of a simulation are influenced not only by the geometry and material properties but also by the shape and size of the mesh. If a curve is made with the horizontal axis being the number of elements and the vertical axis being the simulation result, a logarithmic curve will usually be formed. On the logarithmic curve, the number of elements and the size of the mesh that can be used can be determined. The determination can be made by looking at the number of elements that have started to converge (if the elements are multiplied it does not have a big effect on the result).

In this study, a convergence mesh study is carried out to determine a mesh that can be used for further research on OTEC. In this study, a mesh convergence study was carried out using a step buckle in ABAQUS software. The model used in this study is the model used before. The mesh convergence study carried out in this study was carried out by changing the size of the mesh used. The size of the mesh used is between 50 mm and 200 mm with a distance between 5 mm mesh variations. The results of this mesh convergence study are plotted graphically with the horizontal axis being the number of elements and the vertical axis being the critical moment. The results of the mesh convergence study in this study can be seen in Figure 9.

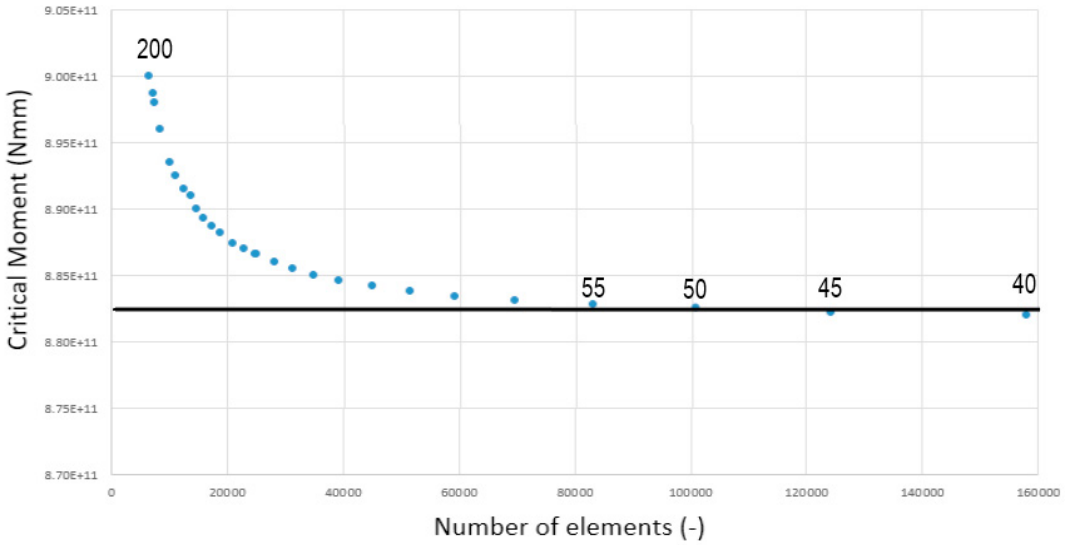


Figure 9. Results of the mesh convergence study.

From the results of the mesh convergence study that has been carried out, a logarithmic curve is obtained (can be seen in Figure 9). From this curve, it can be seen that the more the number of elements, the smaller the critical moment. The greater the number of elements, the more convergent the results obtained. This is shown when a large number of elements have nearly the same value.

In Figure 9, a straight line is drawn which is used to observe where convergence occurs. The trend line indicates that starting with a mesh size of 55 mm if the number of elements is added again, the results of the critical moment are not too influential (can be seen from the affected points with black lines in Figure 9). This shows that the mesh size of 55 mm is ideal for this problem. In addition, a 55 mm mesh size has a smaller number of elements compared to a smaller mesh size, so the numerical calculations performed by the computer are not as many as those on smaller meshes. This shows that the mesh size of 55 mm is the mesh that has the best computational efficiency.

## 5. Conclusions

From the research that has been successfully carried out, it can be concluded that for the numerical validation carried out, the present study and the references used are almost similar with a similarity level of up to 15%. The dissimilarity

that occurs can be due to the material input between the present study and the reference which is not the same. In the stress contour, the propagation is only on one side and in the same direction. This is because the structure only consists of one component, so the direction of stress does not fluctuate. The stress propagation that occurs also only occurs in the middle of the pipe. This causes the strain to only occur in the middle of the pipe. The strain in the middle causes displacement to occur only half the length of the pipe. The next conclusion is that in the mesh convergence study, the size of the mesh that can be used for subsequent research is 55 mm. This is because the mesh size is 55 mm, the results obtained are not too different from the smaller mesh sizes, but there are not too many calculations. Suggestions for future research are to try to simulate the geometries used in CWP OTEC to see the structure's response..

## Acknowledgments

This work was supported by the RKAT PTNBH Universitas Sebelas Maret Year 2023, under the Research Scheme of "Penelitian Kolaborasi Internasional" (KI-UNS), with research grant/contract no. 254/UN27.22/PT.01.03/2023. The support is gratefully acknowledged by the authors.

## References

Adiputra, R., Utsunomiya, T., Koto, J., Yasunaga, T., Ikegami, Y., 2020. Preliminary design of a 100 MW-net ocean thermal energy conversion (OTEC) power plant study case: Mentawai island, Indonesia. Journal of Marine Science and Technology, 25(1), 48-68.

Adiputra, R, Utsunomiya, T., 2019. Stability based approach to design cold-water pipe (CWP) for ocean thermal energy conversion (OTEC). Applied Ocean Research, 92, 101921.

Adiputra, R., Yoshikawa, T., Erwandi, E., 2023. Reliability-based assessment of ship hull girder ultimate strength. Curved and Layered Structures, 10, 20220189.

Arifin, Z., Prasetyo, S.D., Tjahjana, D.D.D.P., Rachmanto, R.A., Prabowo, A.R., Alfaiz, N.F., 2022. The application of $TiO_2$ nanofluids in photovoltaic thermal collector systems. Energy Reports, 8, 1371-1380.

Arifin, Z., Suyitno, S., Tjahjana, D.D.D.P., Juwana, W.E., Putra, M.R.A., Prabowo, A.R., 2020. The Effect of Heat Sink Properties on Solar Cell Cooling Systems. Applied Sciences, 10(21), 7919.

Engels, W., Zabihian, F., 2014, April. Principle and preliminary calculation of ocean thermal energy conversion. In ASEE 2014 Zone I Conference, Bridgeport, United States.

Jay, A., Myers, A.T., Mirzaie, F., Mahmoud, A., Torabian, S., Smith, E., Schafer, B.W., 2016. Large-scale bending tests of slender tapered spirally welded steel tubes. Journal of Structural Engineering, 142(12), 04016136.

Kyriakides, S., Ok, A., Corona, E., 2008. Localization and propagation of curvature under pure bending in steel tubes with Lüders bands. International Journal of Solids and Structures, 45(10), 3074-3087.

Zhang, Z., 2019. Modeling and simulation for cross-sectional ovalization of thin-walled tubes in continuous rotary straightening process. International Journal of Mechanical Sciences, 153, 83-102.

Lee, K.L., Hsu, C.M., Pan, W.F., 2014. Response of sharp-notched circular tubes under bending creep and relaxation. Mechanical Engineering Journal, 1(2), 13-00142.

Li, Z., Shen, K.C., Zhang, X.H., Pan, G., 2022. Buckling of composite cylindrical shells with ovality and thickness variation subjected to hydrostatic pressure. Defence Technology, 18(5), 862-875.

Liu, C.C., 2018. Ocean thermal energy conversion and open ocean mariculture: The prospect of Mainland-Taiwan collaborative research and development. Sustainable Environment Research, 28(6), 267-273.

Polenta, V., Garvey, S.D., Chronopoulos, D., Long, A.C., Morvan, H.P., 2015. Optimal internal pressurization of cylindrical shells for maximising their critical bending load. Thin-Walled Structures, 87, 133-138.

Prabowo, A.R., Prabowoputra, D.M., 2020. Investigation on Savonius turbine technology as harvesting instrument of non-fossil energy: Technical development and potential implementation. Theoretical and Applied Mechanics Letters, 10(4), 262-269.

Prabowoputra, D.M., Hadi, S., Sohn, J.M., Prabowo, A.R., 2020c. The effect of multi-stage modification on the performance of Savonius water turbines under the horizontal axis condition. Open Engineering, 10, 793-803.

Prabowoputra, D.M., Prabowo, A.R., 2022. Effect of the Phase-Shift Angle on the vertical axis Savonius wind turbine performance as a renewable-energy harvesting instrument. Energy Reports, 8, 57-66.

Prabowoputra, D.M., Prabowo, A.R., Bahatmaka, A., Hadi, S., 2020a. Analytical Review of Material Criteria as Supporting Factors in Horizontal Axis Wind Turbines: Effect to Structural Responses. Procedia Structural Integrity, 27, 155-162.

Prabowoputra, D.M., Prabowo, A.R., Hadi, S., Sohn, J.M., 2020b. Assessment of turbine stages and blade numbers on modified 3D Savonius hydrokinetic turbine performance using CFD analysis. Multidiscipline Modeling in Materials and Structures, 17, 253-272.

Timoshenko, S.P., Gere, J.M., 1961. Theory of elastic stability. McGraw-Hill, New York, United States.

Yadav, K.K., Gerasimidis, S., 2019. Instability of thin steel cylindrical shells under bending. Thin-Walled Structures, 137, 151-166.

Yang, M.H., Yeh, R.H., 2014. Analysis of optimization in an OTEC plant using organic Rankine cycle. Renewable Energy, 68, 25-34.

Yudo, H., Yoshikawa, T., 2015. Buckling phenomenon for straight and curved pipe under pure bending. Journal of Marine Science and Technology, 20(1), 94-103.